AD-A094 620 COLD REGIONS RESEARCH AND ENGINEERING LAB HANOVER NH F/G 8/12
MODELING OF ANISOTROPIC ELECTROMAGNETIC REFLECTION FROM SEA ICE--ETC(U)
OCT 80 K M GOLDEN, S F ACKLEY NSF-DPP77-24528
UNCLASSIFIED CRREL-80-23 NL

1 OF 1
AD A094620

END
DATE FILMED
3-81
DTIC

CRREL

LEVEL II

12

Modeling of anisotropic electromagnetic reflection from sea ice

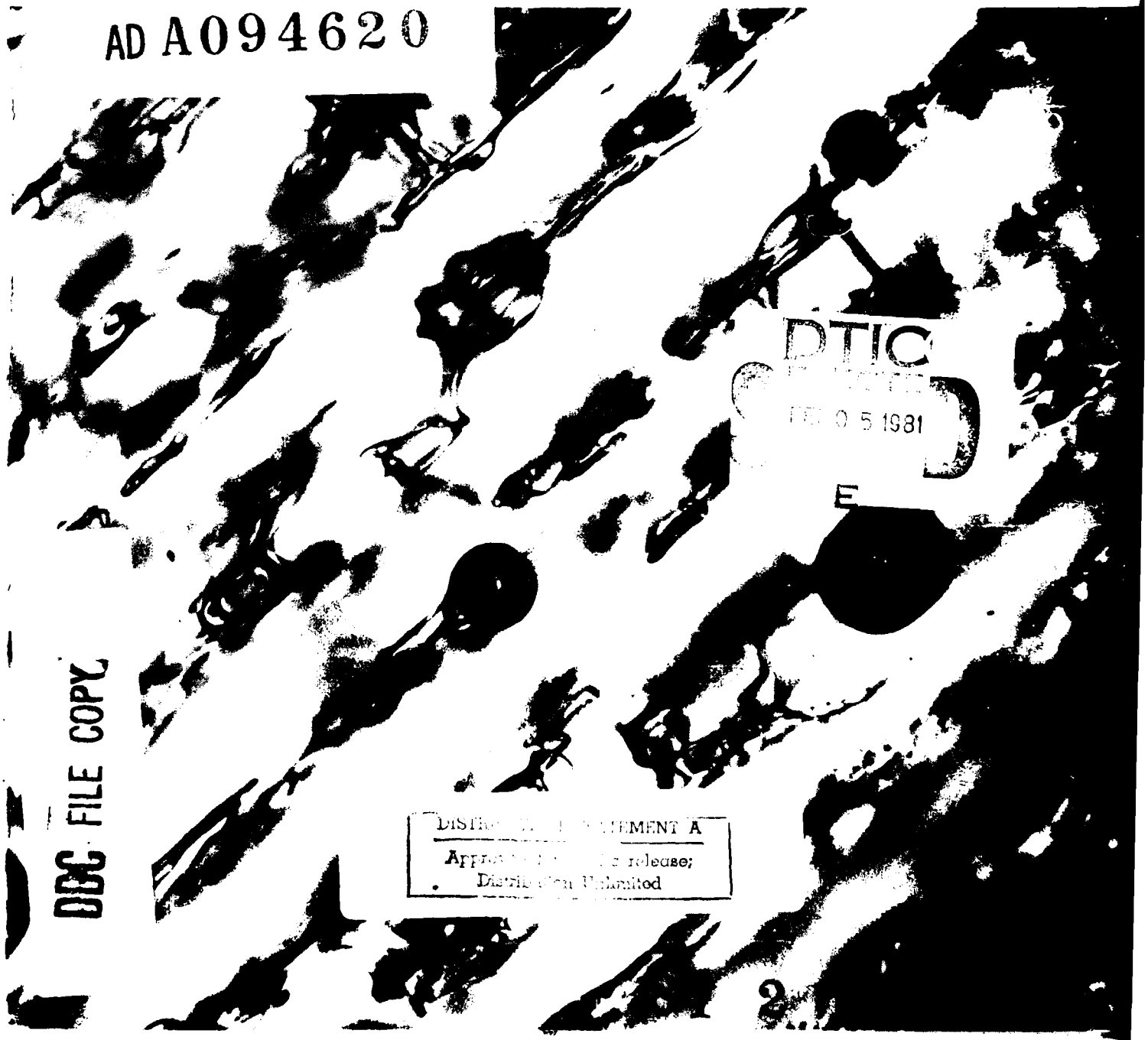

For conversion of SI metric units to U.S. British customary units of measurement consult ASTM Standard E380, Metric Practice Guide, published by the American Society for Testing and Materials, 1916 Race St., Philadelphia, Pa. 19103.

Cover: Photomicrograph of a thin section of sea ice illustrating brine pocket shapes. (Photograph from CRREL Research Report 269 by W. Weeks and A. Assur.)

CRREL Report 80-23

Modeling of anisotropic electromagnetic reflection from sea ice

Kenneth M. Golden and Stephen F. Ackley

October 1980

Prepared for
NATIONAL SCIENCE FOUNDATION
By
UNITED STATES ARMY
CORPS OF ENGINEERS
COLD REGIONS RESEARCH AND ENGINEERING LABORATORY
HANOVER, NEW HAMPSHIRE, U.S.A.

Unclassified

SECURITY CLASSIFICATION OF THIS PAGE (When Data Entered)

REPORT DOCUMENTATION PAGE	READ INSTRUCTIONS BEFORE COMPLETING FORM
1. REPORT NUMBER: CRREL [redacted]80-23	2. GOVT ACCESSION NO.: AD-A094 620
	3. RECIPIENT'S CATALOG NUMBER
4. TITLE (and Subtitle): MODELING OF ANISOTROPIC ELECTROMAGNETIC REFLECTION FROM SEA ICE	5. TYPE OF REPORT & PERIOD COVERED
	6. PERFORMING ORG. REPORT NUMBER
7. AUTHOR(s): Kenneth M. Golden and Stephen F. Ackley	8. CONTRACT OR GRANT NUMBER(s): National Science Foundation, Division of Polar Programs Grant DPP77-24528
9. PERFORMING ORGANIZATION NAME AND ADDRESS: U.S. Army Cold Regions Research and Engineering Laboratory, Hanover, New Hampshire 03755	10. PROGRAM ELEMENT, PROJECT, TASK AREA & WORK UNIT NUMBERS: [illegible]
11. CONTROLLING OFFICE NAME AND ADDRESS: National Science Foundation, Washington, D.C.	12. REPORT DATE: Oct[redacted]1980
	13. NUMBER OF PAGES: 21
14. MONITORING AGENCY NAME & ADDRESS (if different from Controlling Office)	15. SECURITY CLASS. (of this report): Unclassified
	15a. DECLASSIFICATION/DOWNGRADING SCHEDULE

16. DISTRIBUTION STATEMENT (of this Report)

Approved for public release; distribution unlimited.

17. DISTRIBUTION STATEMENT (of the abstract entered in Block 20, if different from Report)

18. SUPPLEMENTARY NOTES

19. KEY WORDS (Continue on reverse side if necessary and identify by block number)

Anisotropy
Electromagnetic wave reflections
Mathematical models
Sea ice

20. ABSTRACT (Continue on reverse side if necessary and identify by block number)

The contribution of brine layers to observed reflective anisotropy of sea ice at 100 MHz is quantitatively assessed. The sea ice is considered to be a stratified, inhomogeneous, anisotropic dielectric consisting of pure ice containing ordered arrays of conducting inclusions (brine layers). Below the transition zone, the ice is assumed to have constant azimuthal c-axis orientation within the horizontal plane, so that the orientation of brine layers is uniform. The brine layers are also assumed to become increasingly well-defined with depth, since adjacent brine inclusions tend to fuse together with increasing temperature. A theoretical explanation for observed reflective anisotropy is proposed in terms of anisotropic electric flux penetration into the brine layers. Penetration anisotropy and brine layer geometry are linked to anisotropy in the complex dielectric constant of sea ice. In order to illustrate the above effects we present a numerical method of

DD FORM 1 JAN 73 1473 EDITION OF 1 NOV 65 IS OBSOLETE

Unclassified

SECURITY CLASSIFICATION OF THIS PAGE (When Data Entered)

20. Abstract (cont'd)

approximating the reflected power of a plane wave pulse incident on a slab of sea ice. Mixture dielectric constants are calculated for two polarizations of the incident wave: 1) the electric field parallel to the c-axis direction, and 2) the electric field perpendicular to the c-axis direction. These dielectric constants are then used to calculate power reflection coefficients for the two polarizations. Significant bottom reflection ($R \approx 0.08$) occurs when the polarization is parallel to the c-axis. However, when the polarization is perpendicular to the c-axis, the return may be almost completely extinguished ($R < 0.001$). This extinction is due primarily to absorptive loss associated with the conducting inclusions and secondarily to an impedance match at the ice/water interface that results in transmission of the wave to the water without reflection.

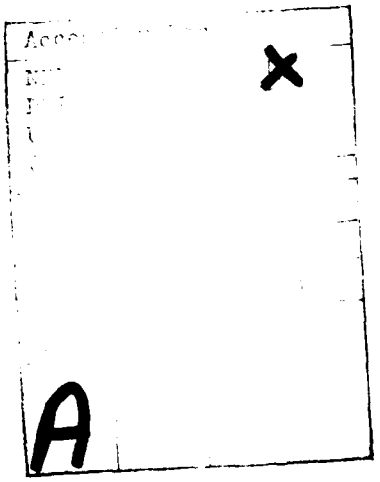

PREFACE

This report was prepared by Kenneth M. Golden, Mathematics Aid, and Stephen F. Ackley, Research Physicist, of the Snow and Ice Branch, Research Division, U.S. Army Cold Regions Research and Engineering Laboratory. Funding for this research was provided by the National Science Foundation, Division of Polar Programs, under Grant DPP77-24528.

The authors would like to thank Dr. Wilford Weeks for supplying salinity and temperature data and for technically reviewing the manuscript, Dr. Anthony Gow for supplying data and general information on sea ice structure, and Dr. Steven Arcone for technical review of the manuscript and consultation on electromagnetic wave propagation.

CONTENTS

ILLUSTRATIONS

TABLES

LIST OF SYMBOLS

a, b, c	principal axes of an ellipsoid in x,y,z-space
da	differential element of a surface area
$\|\|\vec{A}\|\|$	norm of a vector $\vec{A}$
$\vec{B}$	magnetic induction field
$\|C\|$	modulus of a complex number C
d	thickness of sea ice layers
D	directivity of transmitting/receiving antenna
$\vec{D}$	electric displacement field
D_r	directivity of receiving antenna
D_t	directivity of transmitting antenna
E_{1n}	component of electric field in ice normal to brine/ice interface
E_{2n}	component of electric field in brine normal to brine/ice interface
E_{1t}	component of electric field in ice tangential to brine/ice interface
E_{2t}	component of electric field in brine normal to brine/ice interface
$\vec{E}$	applied electric field
$\vec{E} \times \vec{H}$	Poynting vector
$\vec{E}_0, \vec{E}_{2k0}$ $\vec{E}_{20}, \vec{H}_{20}$	vectors constant in space and time
$\vec{E}_{2k}$	electric field inside an ellipsoid due to initially uniform field applied along axis k
$\vec{E}_n$	applied electric field for normal polarization
$\vec{E}_t$	applied electric field for tangential polarization
g_1	conductivity of pure ice
g_2	conductivity of brine
$g_k(i)$	conductivity of layer i for polarization k
h	distance from antenna to interface i
$\vec{H}$	magnetic intensity field
$\vec{J}$	current density field
K	coefficient of anisotropy for net bottom reflection
K^i	coefficient of anisotropy for interfacial bottom reflection
ℓ	number of layers
n	index denoting sea ice/sea water interface ($n = \ell+1$)
$\hat{n}$	outward unit normal vector
n_k	depolarization factor of ellipsoids along axis k
$n_k(i)$	depolarization factor of ellipsoids in layer i for polarization k
$\vec{p}$	dipole moment
$\vec{P}$	polarization field
P_r	power in the load of a receiving antenna
P_t	power radiated by a transmitting antenna
dq	differential element of charge
r	travel distance between transmitting and receiving antennas
$\vec{r}$	position vector
$r_k(i)$	interfacial amplitude reflection coefficient for interface i and polarization k
$R_k(i)$	power reflection coefficient for interface i and polarization k
$R_k^A(i)$	attenuated power reflection coefficient for interface i and polarization k
S_i	salinity of layer i
S	surface of an ellipsoid
$S(i)$	beam spread factor for interface
Δt	plane wave pulse width in time
T	thickness of sea ice
dv	differential element of volume
v_1	velocity of 100 MHz radiation in pure ice
V	volume of an ellipsoid
W	power flowing into ellipsoid per unit volume
W_n	absorbed power density for normal polarization
W_t	absorbed power density for tangential polarization
Z	depth in sea ice
$Z_k(i)$	bulk impedance of layer i for polarization k
$\alpha_k(i)$	attenuation constant of layer i for polarization k
$\gamma_k(i)$	propagation constant of layer i for polarization k
δ	phase difference between electric fields in ice and brine
ϵ_0	permittivity of free space

ϵ_1	complex dielectric constant of host (ice)
ϵ_1'	real part of ϵ_1 (dielectric constant)
ϵ_1''	imaginary part of ϵ_1 (dielectric loss)
ϵ_2	complex dielectic constant of ellipsoids (brine)
ϵ_2'	real part of ϵ_2
ϵ_2''	imaginary part of ϵ_2
$\epsilon_k(i)$	mixture complex dielectric constant of layer i for polarization along k axes of ellipsoids
$\epsilon_k'(i)$	real part of $\epsilon_k(i)$
$\epsilon_k''(i)$	imaginary part of $\epsilon_k(i)$
ϵ_n'	real part of mixture complex dielectric constant for normal polarization
ϵ_n''	imaginary part of mixture dielectric constant for normal polarization
ϵ_t'	real part of mixture complex dielectric constant for tangential polarization
ϵ_t''	imaginary part of mixture dielectric constant for tangential polarization
θ	polar angle of spherical coordinates
θ_i	temperature of layer i
$f(\theta,\phi)$	normalized power pattern
λ	wavelength of radiation
λ_0	free space wavelength
μ_0	permeability of free space
v	relative volume of inclusions
v_b	relative volume of brine in ice
$v_b(i)$	relative brine volume of layer i
ξ	phase difference between magnetic intensity field in brine and electric field in ice
σ_f	free surface charge density
σ_p	bound polarization surface charge density
τ	temporal period of radiation
τ_{cond}	relaxation time for ionic conduction
τ_{water}	relaxation time for water dipole rotations
ϕ	azimuthal angle of spherical coordinates
ω	angular frequency of radiation
$d\Omega$	differential element of solid angle (= $\sin\theta d\theta d\phi$)

MODELING OF ANISOTROPIC ELECTROMAGNETIC REFLECTION FROM SEA ICE

Kenneth M. Golden and Stephen F. Ackley

INTRODUCTION

It has been established that there exists anisotropy in the strength of the return from impulse radar soundings in sea ice (Campbell and Orange 1974, Kovacs and Morey 1978). In this report we quantitatively assess the role of sea ice microstructure in determining the nature of this anisotropy.

Anisotropy and sea ice macrostructure

The amplitude of a radar signal reflected from the ice/water interface may depend markedly on the azimuthal orientation of the linearly polarizing antenna of a radar system with center frequency at 100 MHz (Campbell and Orange 1974). When the antenna is positioned in the horizontal plane parallel to the sea ice surface and rotated about a vertical axis, successive maxima and minima of bottom signal strength are spaced at approximately 90° intervals (Fig. 1). In the most extreme cases of this anisotropy, the signal appears to be completely extinguished. This means, of course, that the signal returned is of such small amplitude that it cannot be distinguished from background noise; i.e. the sensitivity of the receiving instrument has been surpassed.

In addition to anisotropy of bottom reflection, Kovacs and Morey (1978) have observed variation in *surface* reflection, depending on azimuthal orientation of the antenna, when measurements were done at a center frequency of 625 MHz. The anisotropy associated with the ice/air interface at this frequency is, however, much smaller than that associated with the ice/water interface at 100 MHz. There does not seem to be a well-defined relationship between the directions of minimum or maximum bottom and surface reflection. In some cases the directions coincide, in others the difference approaches 90°.

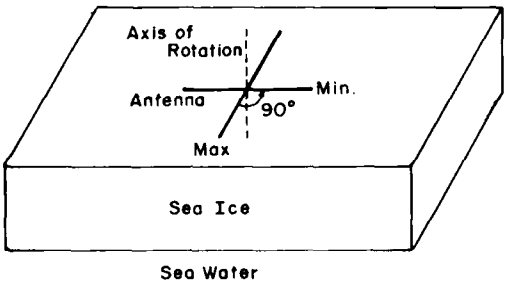

Figure 1. Rotation of antenna to achieve reflective maxima and minima.

Anisotropy of reflection from sea ice has been observed in both first- and multiyear ice with a range in thickness from 25 cm to over 2 m. Freshwater ice has never been observed to exhibit anisotropy (Campbell and Orange 1974). Anisotropy is observed more often in first-year ice than in multiyear ice and is more pronounced in the younger ice. Where first-year ice is smooth and undeformed, the azimuthal orientations of the antenna that correspond to maximum and minimum bottom reflections stay constant over distances of many kilometers. In areas of broken-up or multiyear pack ice consisting of rotated and refrozen floes, the antenna orientations vary drastically over distances of several meters.

Anisotropy and sea ice microstructure

Associated with differences in sea ice macrostructure are differences in microstructure. For example, first-year ice generally has a higher brine content than multiyear ice, because the ice rejects brine with age. We will now review sea ice microstructure and its relation to the reflective anisotropy.

Sea ice is an inhomogeneous anisotropic material

consisting primarily of pure ice surrounding pockets of brine. Tiny spherical crystals of pure ice constitute the first component of newly forming sea ice. These spherical crystals grow rapidly into disks and then into dendritic plates. The plane of a dendritic plate coincides with the basal plane of the ice crystal that comprises it and is perpendicular to the optic or c-axis of the crystal. In calm water, the plates freeze together to form a smooth skim of ice, with c-axis orientation primarily vertical. In turbulent water, the plates are tossed about and broken up so that when they congeal into an ice surface, the c-axis orientation is quite random. As growth continues downward, the c-axes, through a process of geometric selection, become predominantly horizontal. The layer within the ice where the c-axis orientation changes from vertical or random to predominantly horizontal is called the transition zone. This zone is about 10 to 15 cm thick and occurs at a depth anywhere from approximately 2 to 60 cm, depending on growth conditions (Weeks and Assur 1967, Hobbs 1974, Anderson and Weeks 1958, Weeks and Gow 1979).

The ice/water interface where crystal growth takes place is not smooth. When ice forms from sea water, ions (salts) are rejected, since salts are extremely insoluble in ice (Hobbs 1974). The rejection of salts causes an increased solute concentration adjacent to the slowly advancing solid/liquid interface. This increased concentration of salt and an appropriate temperature profile produce a zone of constitutionally supercooled liquid below the interface (Weeks and Gow 1979). Tiller (1974) has indicated that the type of solid/liquid interface associated with constitutionally supercooled liquid is dendritic or cellular, rather than planar. Thus, the dendritic plates perpendicular to the c-axes are elongated parallel to their basal planes and extend into the sea water below (Fig. 2). As further growth occurs, the concentrated sea water between the dendritic plates becomes trapped and makes up the so-called brine layers of sea ice. Since the c-axis is perpendicular to the longer dimensions of the dendritic plates, it must also be perpendicular to the longer dimensions of the brine layers.

Immediately above the ice/water interface, the ice is relatively warm and contains a high concentration of brine layers (Fig. 3a). The spacing between adjacent layers is the thickness of a dendritic plate. Farther up the temperature decreases and, consequently, the brine layers begin to "neck" (Fig. 3b) and change into rows of closely spaced cylinders (Fig. 3c), and finally into elliptical cylinders (Fig. 3d). Below the transition zone, the layers or rows stand up vertically with the shortest dimension horizontal. Above the transition zone, the arrangement is more random

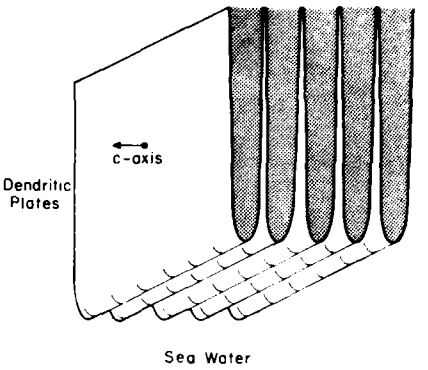

Figure 2. Dendritic plates at ice/water interface, elongated parallel to their basal planes, extending into the sea water below. Sea water trapped between the plates becomes the brine layers (from Weeks and Gow 1979).

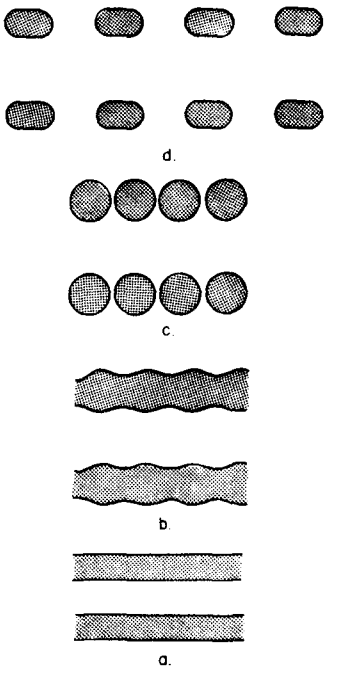

Figure 3. Brine layers (top view) near the bottom of sea ice (a) begin to "neck" with decreasing temperature farther up in the ice sheet (b) and freeze out into cylinders (c) and elliptical cylinders (d) (from Anderson and Weeks 1958).

depending on growth conditions. This model of brine structure is, of course, idealized. Brine drainage influenced by gravity and temperature gradient is but one factor that could alter the idealized model.

Below the transition zone the c-axes lie predominantly in the horizontal plane. Accordingly, layers of brine in each crystal grain are positioned with their two longer dimensions lying in a vertical plane perpendicular to the c-axis, and with their short dimension oriented horizontally and parallel to the c-axis. Recent studies of arctic fast ice (Cherepanov 1971, Weeks and Gow 1979, Kovacs and Morey 1978) have shown that the c-axes not only have a preferred horizontal orientation, but also have a preferred *azimuthal* direction within the horizontal plane. Cherepanov (1971) found the azimuthal c-axis alignment to be constant for hundreds of kilometers in the Kara Sea. Weeks and Gow (1979) and Kovacs and Morey (1978) found good positive correlation between the preferred direction of c-axis azimuth and "long term" current direction beneath the growing ice. Weeks and Gow (1979) proposed an explanation for the preferred orientation in terms of these currents.

Preferred azimuthal orientation of c-axes corresponds to preferred azimuthal orientation of brine layers. Therefore, in the bottom portions of undeformed ice, we expect ordered arrays of brine layers with uniform alignment over a large area. This ordered arrangement of c-axes and brine layers is apparently related to the reflective anisotropy. Campbell and Orange (1974) and Kovacs and Morey (1978) have found that a maximum reflection from the ice/water interface occurs when the electromagnetic wave is polarized so that the direction of the electric field parallels the preferred c-axis direction, or equivalently, when it is polarized so that the electric field is normal to the principal brine/ice interface (normal polarization). The minimum reflection from the ice/water interface occurs when the pulse is polarized so that the direction of the electric field is perpendicular to the preferred c-axis direction, or, equivalently, the electric field is tangential to the principal brine/ice interface (tangential polarization). These findings suggest at least two sources for the observed reflective anisotropy: 1) uniform crystal arrangement and 2) uniform brine layer arrangement. Hargreaves (1977) has found that anisotropy of reflection due to oriented crystals is much smaller than that found in sea ice. Thus, we reject uniform crystal arrangement as the primary cause of the reflective anisotropy and will offer a theoretical explanation for the observed reflective anisotropy of sea ice in terms of the ordered arrays of brine layers.

A THEORY OF ANISOTROPIC RADAR RETURN FROM SEA ICE

We propose that the asymmetrical geometry of the brine layers causes an anisotropy in the penetration of the impinging electric field into the brine inclusions. This anisotropic penetration is associated with an anisotropy in the effective complex dielectric constant of the sea ice, which determines the power returned to the receiver.

Anisotropic electric flux penetration into brine layers

To illustrate the proposed anisotropic behavior of the field, we take the following values as the dimensions of a representative bottom sea ice brine layer. Anderson and Weeks (1958) give the horizontal thickness b of a typical brine layer as 0.1 mm. Kovacs and Morey (1978) give the vertical length c of a brine layer as $5b$. The horizontal length a of a brine layer perpendicular to the c-axis, determined by examination of rubbings from sea ice bottom cores (Weeks and Assur 1967), is typically 3 mm. An idealized model of a brine layer is a non-degenerate ellipsoid ($a > c > b$) with a surface defined by

$$\frac{x^2}{a^2} + \frac{y^2}{b^2} + \frac{z^2}{c^2} = 1 \qquad (1)$$

where a = 3 mm, b = 0.1 mm, and c = 0.5 mm. The x-axis is horizontal and perpendicular to the crystal optic axis, the y-axis is horizontal and parallel to the optic axis, and the z-axis is vertical. This analytical form allows approximation of electric flux penetration into a brine layer.

Tinga et al. (1973) derive an expression for the electric field $\vec{E}_{2k}$ inside a member of a set of ellipsoidal inclusions (brine) of complex dielectric constant ϵ_2, relative volume v, and uniform axial alignment, dispersed in a homogeneous medium (ice) of complex dielectric constant ϵ_1, subjected to an initially uniform electric field $\vec{E}$ directed along one of the principal axes $k = a, b, c$:

$$\vec{E}_{2k} = \frac{\epsilon_1}{\epsilon_1 + n_k(1-v)(\epsilon_2 - \epsilon_1)}\vec{E} \qquad (2)$$

where

$$n_k = \frac{abc}{2}\int_0^\infty \frac{ds}{(k^2+s)\sqrt{(a^2+s)(b^2+s)(c^2+s)}} \qquad (3)$$

is called the depolarization factor (Stratton 1941) of the ellipsoid along the axis k, and depends only on the axial ratios. Note that the field inside the ellipsoid is uniform. The applicability of this equation to the calculation of electric fields inside a brine layer (of largest dimension a) at 100 MHz depends primarily on the condition that $a \ll \lambda$, which is satisfied for the wavelength $\lambda = 1.7$ m in pure ice. In addition, since brine volumes (relative volume of brine to ice) near the bottom of sea ice reach 0.4 and the electric field inside a brine layer is influenced by the dipole fields of its neighbors, the derivation of the equation should include interaction effects. In the self-consistent multiphase dielectric mixture theory developed by Tinga et al. (1973), an extra boundary has been introduced between the inclusions to account for these effects to first order.

We assume the electric fields are of the form $\vec{E}(t) = \vec{E}_0 e^{-j\omega t}$ and $\vec{E}_{2k}(t) = \vec{E}_{2k0} e^{-j(\omega t+\delta)}$ with no spatial dependence, where $j = \sqrt{-1}$, $\omega = 2\pi \times 10^8$ rad/s and δ is the phase difference between fields. We evaluate eq 2 for the two cases of interest, $k = a$ and $k = b$, where $n_a = 9.67\times 10^{-3}$ and $n_b = 8.39\times 10^{-1}$ are calculated by numerical integration. We take $\epsilon_1 = \epsilon_1' + j\epsilon_1'' = 3.17 + j0.013$ (Johari and Charette 1975) and $\epsilon_2 = \epsilon_2' + j\epsilon_2'' = 80 + j1000$ (Vant 1976), and set $v = v_b = 0.29$, where $v_b = 0.29$ is the brine volume at 5 cm from the bottom of a piece of arctic sea ice, as obtained from a polynomial fit of brine volume data.

Case 1. Normal polarization, applied field $\vec{E} = \vec{E}_n \| b$

Taking the real part of $E_{2b} = ||\vec{E}_{2b0}|| e^{-j(\omega t+\delta)}$ to be the physical scalar field (Jackson 1975), we obtain from eq 2

$$\mathrm{Re}(E_{2b}) = (4.49\times 10^{-4})\,\mathrm{Re}(E_n) - (5.20\times 10^{-3})\,\mathrm{Im}(E_n) \quad (4)$$

where the mixing of the real and imaginary parts of E indicates a phase shift, with $\delta = \tan^{-1}(5.20\times 10^{-3}/4.49\times 10^{-4}) = 85.1°$. The moduli of the complex scalar fields, or equivalently the amplitudes of the physical fields, satisfy

$$|E_{2b}| = \left(\frac{4.49\times 10^{-4}}{\cos\delta}\right)|E_n| = (5.26\times 10^{-3})\,|E_n|. \quad (5)$$

Therefore, the electric field is *excluded* from the brine layer for normal polarization. Mathematically, this exclusion arises from the boundary condition on the normal component of a harmonically time-dependent electric field at the interface between two media,

$$E_{2n} = \left(\frac{j\epsilon_1' - \epsilon_1''}{j\epsilon_2' - \epsilon_2''}\right) E_{1n} \approx \frac{\epsilon_1}{\epsilon_2} E_{1n}. \quad (6)$$

Everywhere on the brine/ice interface the *normal component* of the field in the brine must be very small compared to that in ice, $|E_{2n}| = (3.16\times 10^{-3})|E_{1n}|$. During normal polarization, the surface of the brine layer is primarily normal to the applied field so that the uniform field *inside* the brine layer must be of a very small magnitude. Physically, this exclusion arises from a large depolarizing field within the brine layer created by the buildup of free (ionic) charges and bound polarization charges (from water dipole rotations) on the principal interface so that the net field inside the brine layer is very small. The existence of these effects is supported by the fact that the relaxation times in brine for ionic conduction $\tau_{cond} = \epsilon_2'/\omega\epsilon_2'' \approx 1.3\times 10^{-10}$ s (Stratton 1941) and water dipole rotations $\tau_{water} \approx 2\times 10^{-11}$ s (Vant 1976) are both significantly shorter than $\tau/2 = 5\times 10^{-9}$ s, where τ is the temporal period of a 100-MHz wave.

Case 2. Tangential polarization, applied field $\vec{E} = \vec{E}_t \| a$

Taking the real part of E_2 to be the physical scalar field, we obtain for tangential polarization from eq 2,

$$\mathrm{Re}(E_{2a}) = (1.90\times 10^{-1})\,\mathrm{Re}(E_t) - (3.54\times 10^{-1})\,\mathrm{Im}(E_t) \quad (7)$$

with $\delta = \tan^{-1}(3.54\times 10^{-1}/1.90\times 10^{-1}) = 61.8°$. The moduli of the complex fields, or equivalently the amplitudes of the physical fields, satisfy

$$|E_{2a}| = \left(\frac{1.90\times 10^{-1}}{\cos\delta}\right)|E_t| = (4.01\times 10^{-1})\,|E_t|. \quad (8)$$

Therefore, there is a significant *penetration* of nearly half the applied field into the inclusion for tangential polarization. Mathematically, the penetration arises from the boundary condition that the tangential component of the electric field must be continuous across the brine/ice interface,

$$E_{1t} = E_{2t}. \quad (9)$$

During tangential polarization, the surface of the brine layer is primarily tangential to the applied field, so that

a significant amount of flux penetrates. Physically, penetration, or more accurately the absence of a large depolarizing field, occurs because the field is directed *along* the interface over most of the surface causing adjacent polarization charges to cancel and free charges to travel (though certainly not far) rather than accumulate. The field cannot penetrate completely, however, since there is a small depolarizing field created by the buildup of charges at the ends of the brine layer.

Implications of normal exclusion, tangential penetration, and brine layer geometry for dielectric behavior of sea ice

Absorption

Let S be the surface of an (ellipsoidal) brine layer V and $\vec{E}$, $\vec{H}$, $\vec{E}_2$, $\vec{H}_2$, $\vec{D}_2$, $\vec{B}_2$, and $\vec{J}_2$ be the physical fields on S and in the brine layer. Then we assume that $\vec{E} = \vec{E}_0 \cos(\omega t)$, $\vec{E}_2 = \vec{E}_{20} \cos(\omega t + \delta)$ and $\vec{H}_2 = \vec{H}_{20} \cos(\omega t + \xi)$ with appropriate dependences for $\vec{D}_2$, $\vec{J}_2$, and $\vec{B}_2$, where, in general, $\delta \neq \xi$. Maxwell's equations may be manipulated (Lorrain and Corson 1970) to yield a statement of energy conservation (or continuity of energy flow),

$$-\int_S \vec{E}\times\vec{H}\cdot\hat{n}\,da = \frac{1}{2}\frac{d}{dt}\int_V (\vec{E}_2\cdot\vec{D}_2+\vec{H}_2\cdot\vec{B}_2)\,dv + \int_V \vec{J}_2\cdot\vec{E}_2\,dv \qquad (10)$$

where $\hat{n}$ is an outward unit normal vector. The rate at which energy (represented by the Poynting vector) flows *into* the brine layer is equal to the increase in electromagnetic field energy stored in the brine layer per unit time plus the energy removed by conversion to heat (conduction losses) per unit time. If one assumes that the brine is linear, isotropic, ohmic and non-magnetic, and that the fields are uniform inside the brine, then eq 10 becomes

$$\begin{aligned}-\int_S \vec{E}\times\vec{H}\cdot\hat{n}\,da &= \frac{V}{2}\left[\frac{d}{dt}(\epsilon'_2\epsilon_0 E_2^2+\mu_0 H_2^2)+g_2 E_2^2\right] \\ &= -\omega V[\epsilon'_2\epsilon_0 E_{20}^2\cos(\omega t+\delta)\sin(\omega t+\delta) \\ &\quad +\mu_0 H_{20}^2\cos(\omega t+\xi)\sin(\omega t+\xi) \\ &\quad +g_2 E_{20}^2\cos^2(\omega t+\delta)] \qquad (11)\end{aligned}$$

where $\mu_0 = 4\pi\times10^{-7}$ N/A^2 is the permeability of free space, $\epsilon_0 = 8.854\times10^{-12}$ C^2/N m^2 is the permittivity of free space, and g_2 is the conductivity of brine in mho/m. If this equation is divided by V and time-averaged over an integral number of periods, then the first two terms on the right side vanish since sine and cosine are orthogonal, and we are left with

$$W = \frac{1}{2} g_2 E_{20}^2 \qquad (12)$$

where we have replaced the time-averaged surface integral with W, the power flowing into the volume V, measured in W/m^3. For tangential polarization, $E_{20} = 4.01\times10^{-1} E_0$; for normal polarization $E_{20} = 5.26\times10^{-3} E_0$. Therefore, the ratio of the power losses is

$$\frac{W_t}{W_n} = \frac{\frac{1}{2}g_2(4.01\times10^{-1})^2 E_0^2 V+\frac{1}{2}g_1 E_0^2 (V/v_b)}{\frac{1}{2}g_2(5.26\times10^{-3})^2 E_0^2 V+\frac{1}{2}g_1 E_0^2 (V/v_b)} \approx 2200 \qquad (13)$$

where we assume that g_1 is the conductivity of pure ice and that the amplitude of the field in the ice is equal to E_0.

In other words, we expect a very large difference in power absorbed by bottom sea ice for the two polarizations. The variation is caused by anisotropy of electric flux penetration into the brine layers, which in turn is related to anisotropy in the amount of brine layer surface situated normal to the electric field.

Because the tangentially polarized wave "sees" (penetrates) the brine layers but the normally polarized wave does not, significant conduction currents are set up throughout the brine layer during tangential polarization but not during normal polarization. Note that we are primarily considering conduction effects, since 100 MHz is below the resonant frequency for water dipole rotations. Thus, for normal polarization, there is a small imaginary mixture dielectric constant ($\epsilon''_n \propto W_n$) with a significant signal transmitted through the medium and subsequently returned to the receiver. For tangential polarization there is a large imaginary mixture dielectric constant ($\epsilon''_t \propto W_t$) with higher attenuation and much less signal returned.

Polarizability

In addition to anisotropic absorption of the wave, the asymmetry of the brine inclusions causes anisotropy in the polarizability of the sea ice, and consequently in the real part of the effective dielectric constant. The dipole moment, defined (Reitz and Milford 1967) by

$$\vec{p} = \int \vec{r}\,dq \qquad (14)$$

for a brine layer with surface S takes the form

$$\vec{p} = \int_S \vec{r}\,(\sigma_f + \sigma_p)\,da \qquad (15)$$

where σ_f is the free (ionic) surface charge density, σ_p is the bound (water dipole rotation) polarization surface charge density, $\vec{r}$ is a position vector, and da is a differential element of charge. During tangential polarization, σ_f and σ_p contribute to the integral in eq 14 primarily when $\vec{r}$ is very large, so that the dipole moment $\vec{p}$ of the brine layer is large. During normal polarization, when the applied field parallels the short axis, σ_p and σ_f are distributed more evenly, so that the dipole moment of the brine layer is smaller. [See van de Hulst (1957) for calculations of these dipole moments for the two polarizations.] The dipole moments $\vec{p}$ of the medium determine its polarization $\vec{P}$, which is related to the real dielectric constant by $\vec{P} = \epsilon_0(\epsilon' - 1)\vec{E}$. Therefore, for tangential polarization there is a larger real dielectric constant than for normal polarization.

We hope that the preceding discussion provides a physical basis for understanding the observed reflective anisotropy. We feel that the complex interplay among the effects described and their relative contributions to the reflective anisotropy is best examined with a numerical model of sea ice reflections, which we will now present.

MODELING OF ELECTROMAGNETIC REFLECTION FROM A STRATIFIED, ANISOTROPIC, INHOMOGENEOUS LOSSY MEDIUM

We wish to obtain reflection profiles of sea ice of thickness T, i.e. graphs of power reflection coefficients (power received from a given depth/power transmitted) vs depth, for the two polarizations of interest. The sea ice is assumed to be composed of layers of uniform thickness d, which we shall take as 10 cm, where the number of layers is $\ell = T/d$. ("Layer" here denotes a particular depth interval, e.g. 150 to 160 cm.) To obtain a reflection profile, we calculate complex dielectric constants $\epsilon_k(i)$ for each layer i, where $i = 1, 2, \ldots, \ell$, and for each polarization, normal and tangential. These dielectric constants (which are actually the first two components of the diagonal dielectric tensor) are used in a calculation of interfacial power reflection coefficients $R_k^I(i)$, where $i = 1, 2, \ldots, n$ and $n = \ell + 1$. $R_k^I(1)$ denotes reflection from the air/ice interface and $R_k^I(n)$ denotes reflection from the ice/water interface. The interfacial power reflection coefficients are used in a calculation of bulk power reflection coefficients $R_k^B(i)$ where $i = 1, 2, \ldots, n$, since, for example, what the receiver measures as the bottom reflection is influenced by the top reflection. These bulk power reflection coefficients are then used to calculate attenuated power reflection coefficients $R_k^A(i)$, where $i = 1, 2, \ldots, n$. This calculation takes losses (attenuation) into account, as determined by the $\epsilon_k(i)$. Finally, the power reflection coefficients $R_k(i)$ are calculated from the $R_k^A(i)$ by including the effect of beam spreading. The reflective behavior of the radar pulse of small width in frequency space is approximated by analysis of the center frequency (100-MHz) component of a plane wave pulse.

Calculation of mixture complex dielectric constants

Tinga et al. (1973) derive an expression for the complex dielectric constant ϵ_k of a mixture consisting of ellipsoids (brine) of complex dielectric constant ϵ_2, relative volume v, and uniform axial alignment, dispersed in a homogeneous medium (ice) of complex dielectric constant ϵ_1 when the mixture is subjected to an initially uniform electric field directed along one of the principal axes $k = a, b, c$ of the ellipsoids:

$$\epsilon_k = \epsilon_1 + \left[\frac{v\epsilon_1(\epsilon_2 - \epsilon_1)}{n_k(1-v)(\epsilon_2 - \epsilon_1) + \epsilon_1}\right] \qquad (16)$$

where n_k is the depolarization factor of the ellipsoid along axis k. Since we consider the sea ice to be stratified, eq 16 takes the form

$$\epsilon_k(i) = \epsilon_1 + \left\{\frac{v_b(i)\,\epsilon_1(\epsilon_2 - \epsilon_1)}{n_k(i)[1 - v_b(i)](\epsilon_2 - \epsilon_1) + \epsilon_1}\right\}$$

$$= \epsilon_k'(i) + j\epsilon_k''(i) \qquad (17)$$

where the brine volume $v_b(i)$ and depolarization factors $n_k(i)$ of the ellipsoids are varied for each layer i to account for the change in physical properties of the ice with depth, and k denotes polarization, either tangential t or normal n. Equation 17 is evaluated using appropriate frequency-dependent values for ϵ_1 and ϵ_2. We assume that the dielectric constants of the ice and brine, ϵ_1 and ϵ_2, are constant with depth. See Vant (1976) for a discussion of the applicability of eq 17 to time-varying fields.

The brine volume $v_b(i)$ is varied according to polynomial fits of data calculated from salinity and temperature profiles obtained from arctic fast ice by W.F. Weeks and A.J. Gow.* Data are considered from Cape Krusenstern, Barrow (Chukchi Sea) and Harrison Bay. The

*W.F. Weeks and A.J. Gow, CRREL, personal communication, 1979.

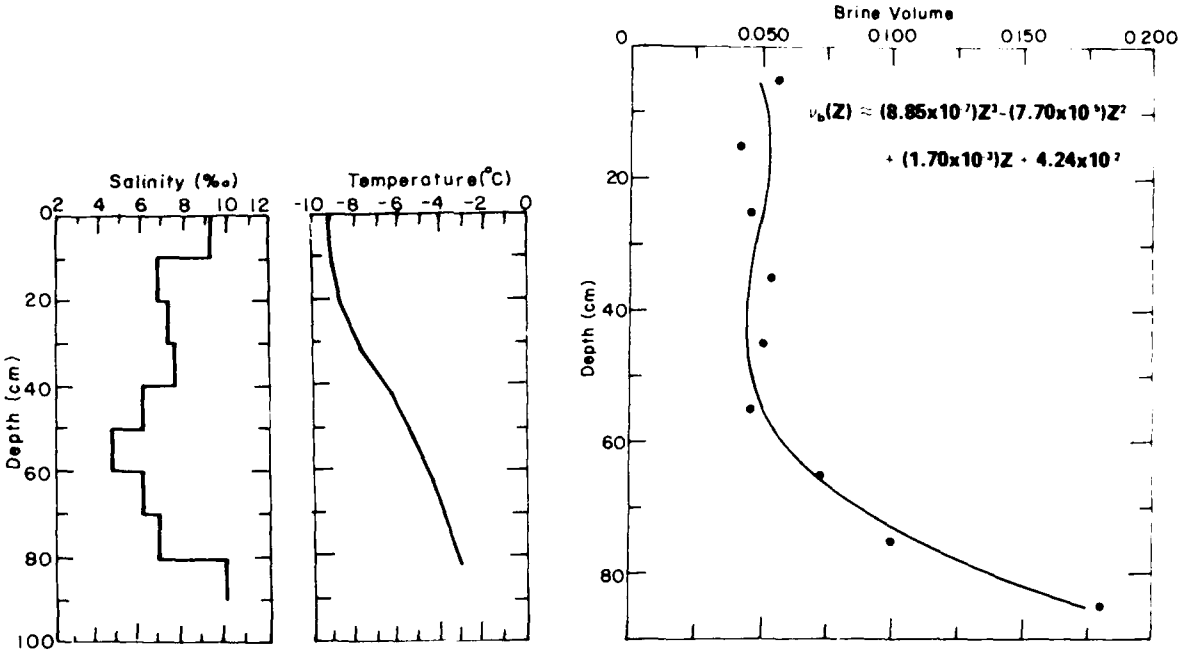

a. Salinity and temperature.

b. Calculated brine volume data with polynomial fit (Z denotes depth.

Figure 4. Salinity, temperature and calculated brine volume data for Cape Krusenstern.

salinity and temperature profiles for the three sites are shown in Figures 4a, 5a and 6a, and the brine volume profiles are shown in Figures 4b, 5b and 6b. For a given 10-cm layer i, the brine volume $v_b(i)$ is calculated using the equation of Frankenstein and Garner (given in Weeks and Assur 1967),

$$v_b(i) = \frac{S_i}{10^3}\left[\frac{-49.185}{\theta_i} + 0.532\right] \qquad (18)$$

where S_i is the salinity of layer i expressed in parts per thousand, θ_i is the temperature of layer i expressed in degrees Celsius, and $v_b(i)$ is expressed as a dimensionless ratio. Polynomial fits were taken to smooth the discontinuities imposed by the sampling procedure, as well as to allow for variation of the layer thickness d.

Recall that a depolarization factor for a particular axis depends only on the axial ratios of the ellipsoid. Thus, we vary the $n_k(i)$ with depth by changing the relationships between the axes. In the bottom 10 cm, we take the relationships to be determined by $a:b:c$ = 30:1:5, so as to model the well-defined brine layers. Throughout the ice sheet we keep b constant but vary a and c linearly so that $a:b:c$ = 1:1:0.5 at the top of the ice sheet. The linear change in the ratio a/b is to simulate the necking and subsequent freezing-out of the brine layers (Fig. 3) with a limit of randomly dispersed tubules ($a = b$) at the top. The vertical (c) dimension is decreased to a value less than $a = b$ at the top to indicate that the longest dimensions of the randomly dispersed tubules have a tendency to be horizontal. Therefore, at the top of the ice there are fat, round disks whose shortest dimension is vertical, and at the bottom there are flat, elongated disks whose shortest dimension is horizontal. At present, very little information is available concerning the detailed geometry of brine structure. The model we use is a rough first order (linear) approximation designed only to reflect the gross features of brine structure: anisotropy near the bottom and isotropy near the top.

Calculation of interfacial power reflection coefficients

We will now calculate interfacial power reflection coefficients $R_k'(i)$ (power reflected by interface i/power incident on interface i) at each interface i for the two polarizations. The characteristic bulk impedance $Z_k(i)$ of layer i for polarization along axis k is defined (Ward 1967) by

$$Z_k(i) = \frac{i\mu_0\omega}{\gamma_k(i)} \qquad (19)$$

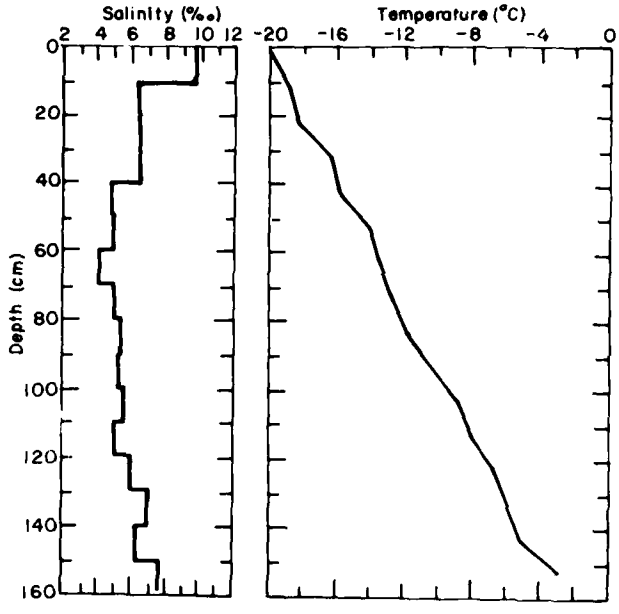

a. Salinity and temperature.

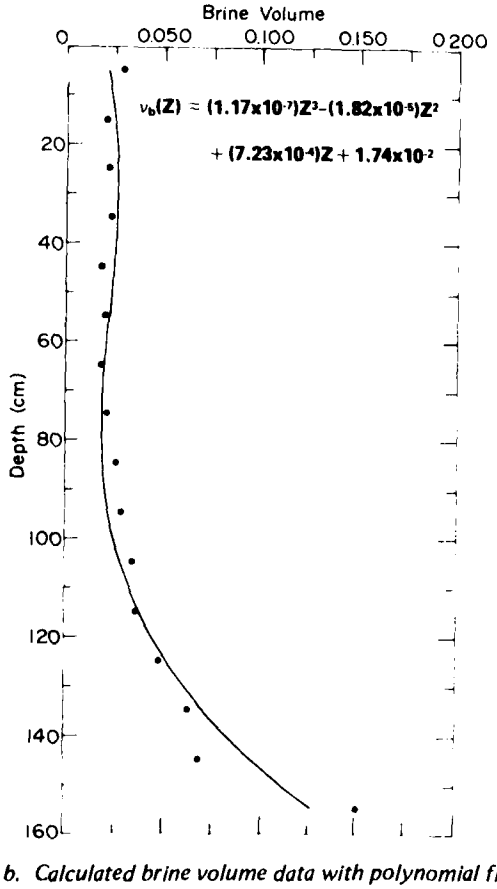

b. Calculated brine volume data with polynomial fit.

Figure 5. Salinity, temperature and calculated brine volume data for Barrow (Chukchi Sea).

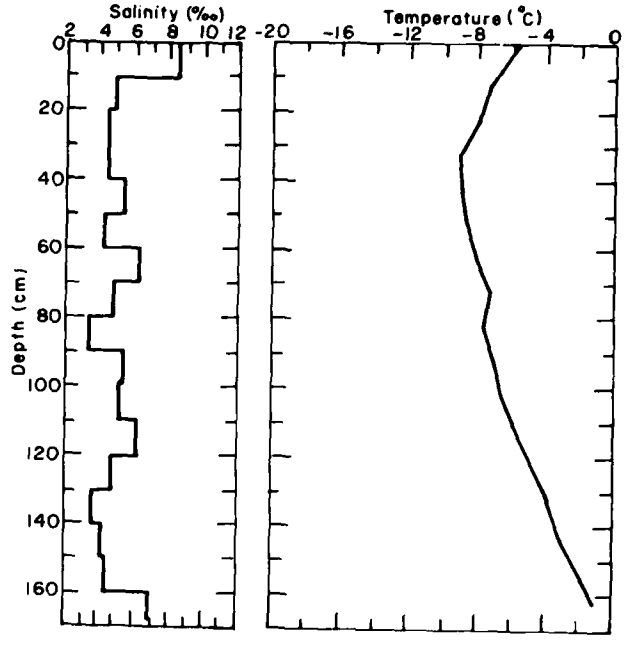

a. Salinity and temperature.

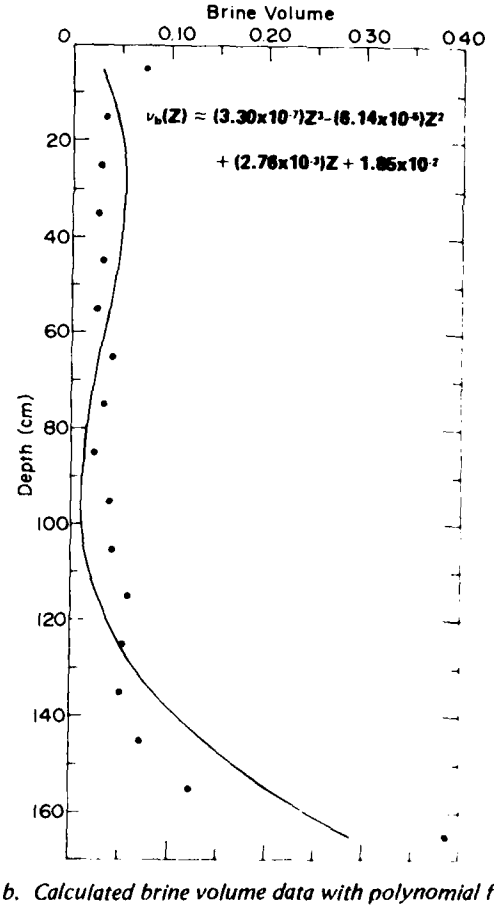

b. Calculated brine volume data with polynomial fit.

Figure 6. Salinity, temperature and calculated brine volume data for Harrison Bay.

where $\gamma_k(i)$ is the propagation constant of layer i defined by

$$\gamma_k(i) = \sqrt{\epsilon_0\mu_0\omega^2\epsilon_k'(i) + j\mu_0\omega g_k(i)}, \qquad (20)$$

$g_k(i)$ is the conductivity of layer i for polarization along the k axis of the ellipsoids, and $\omega = 2\pi\times 10^8$ rad/s. Since we assume that the losses in sea ice at 100 MHz are primarily due to conduction effects, i.e. $g_k(i) = \epsilon_0\omega\epsilon_k''(i)$, eq 20 becomes

$$\gamma_k(i) = \omega\sqrt{\epsilon_0\mu_0\epsilon_k(i)}\ . \qquad (21)$$

The complex *amplitude* reflection coefficient $r_k(i)$ at an interface i depends upon the mismatch of the bulk impedance $Z_k(i-1)$ of layer $i-1$ above the interface and the bulk impedance $Z_k(i)$ of layer i below the interface:

$$r_k(i) = \frac{Z_k(i-1) - Z_k(i)}{Z_k(i-1) + Z_k(i)}. \qquad (22)$$

On substitution of eq 19 and 21 this becomes

$$r_k(i) = \frac{\sqrt{\epsilon_k(i)} - \sqrt{\epsilon_k(i-1)}}{\sqrt{\epsilon_k(i)} + \sqrt{\epsilon_k(i-1)}}. \qquad (23)$$

Note that this expression depends on frequency only through the dispersive nature of the dielectric constants of the constituents of the system, sea water, ice, brine, and air. Finally, the interfacial *power* reflection coefficient $R_k^I(i)$ at interface i is obtained from the complex amplitude coefficient through

$$R_k^I(i) = r_k(i)^* r_k(i) \qquad (24)$$

where * denotes complex conjugation.

Calculation of bulk power reflection coefficients

Consider a homogeneous slab of pure ice (assumed lossless) of thickness d lying below a homogeneous half-space of air and above a homogeneous half-space of sea water. Let a plane wave pulse of duration Δt traveling through air be normally incident on interface 1. Further assume that $\Delta t \ll d/v_1$, where v_1 is the wave velocity in ice. The primary pulse returned to the air from interface 2 has the following bulk power reflection coefficient (power returned to air by the interface/power incident on ice slab, without attenuation):

$$R^B(2) = [1-R^I(1)]\cdot R^I(2)\cdot[1-R^I(1)].$$

A secondary pulse reflected back into the air by interface 2 has the following bulk power reflection coefficient:

$$R^B(2) = [1-R^I(1)]\cdot R^I(2)\cdot R^I(2)\cdot[1-R^I(1)].$$

There are infinitely many of these reflections. For our model of a multi-layered slab of sea ice we neglect multiple reflection effects beyond first order and consider only primary reflections, so that the bulk power reflection coefficient of interface m for polarization k is given by

$$R_k^B(m) = \prod_{i=1}^{m-1}[1-R_k^I(i)]^2\, R_k^I(m) \qquad (25)$$

for $m = 2, 3, \ldots, n$, and

$$R_k^B(m) = R_k^I(m) \qquad (26)$$

for $m = 1$. Figure 7 gives a schematic of the situation.

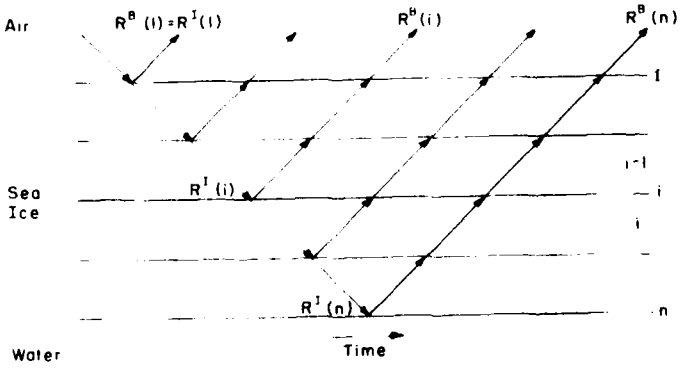

Figure 7. Schematic diagram for bulk power reflection coefficient calculation.

Calculation of attenuated power reflection coefficients

The attenuated power reflection coefficient $R_k^A(i)$ for interface i (power returned to air by interface i/power incident on ice slab) is calculated from $R_k^B(i)$ by including losses from travel through the sea ice. The amplitude of a plane monochromatic wave traveling one way through a lossy layer i of sea ice of thickness d and complex dielectric constant $\epsilon_k(i)$ is decreased by the factor $e^{-\alpha_k(i)d}$, where $\alpha_k(i)$ is defined by von Hippel (1954) as

$$\alpha_k(i) = \frac{2\pi}{\lambda_0}\left(\frac{\epsilon_k'(i)}{2}\left\{\sqrt{1+[\epsilon_k''(i)/\epsilon_k'(i)]^2}-1\right\}^{1/2}\right) \quad (27)$$

where λ_0 is the free space wavelength, and k indicates polarization. One-way power, therefore, decreases by a factor $[e^{-\alpha_k(i)d}]^2$, which may be termed a power transmission coefficient for *layer i*, and we define the attenuated power reflection coefficients $R_k^A(m)$ by

$$R_k^A(m) = \prod_{i=1}^{m-1}[e^{-\alpha_k(i)d}]^4 R_k^B(m) \quad (28)$$

for $m = 2, 3, \ldots, n$, and

$$R_k^A(m) = R_k^I(m) \quad (29)$$

for $m = 1$.

Beam spread

We estimate beam spreading effects with the Friis transmission formula (Kraus 1953), which gives the ratio of the power in the load of a receiving antenna P_r to the power radiated by a transmitting antenna P_t in terms of the distance between the antennas r, the wavelength λ, and the directivities of the transmitting and receiving antenna, D_t and D_r, respectively,

$$\frac{P_r}{P_t} = D_r D_t \left(\frac{\lambda}{4\pi r}\right)^2. \quad (30)$$

The directivity can be expressed as

$$D = \frac{4\pi}{\int f(\theta,\phi)\, d\Omega} \quad (31)$$

where $f(\theta,\phi)$ is the normalized power pattern. For simplicity we assume that the transmitting/receiving antenna in our study radiates energy uniformly over a cone subtending a total polar angle of 90°. The directivity $D = D_r = D_t$ then becomes

$$D = \frac{4\pi}{\int_0^{2\pi} d\phi \int_0^{\pi/4} \sin\theta\, d\theta} \approx 6.83. \quad (32)$$

To obtain the final power reflection coefficients $R_k(i)$, we multiply each $R_k^A(i)$ by the beam spread factor $S(i)$,

$$R_k(i) = S(i)\, R_k^A(i) \quad (33)$$

with

$$S(i) = \frac{P_r(i)}{P_t} = \left(\frac{6.83\lambda}{4\pi \cdot 2h}\right)^2 \quad (34)$$

where h is the distance from the antenna to interface i. Since reflection measurements are often done with the antenna resting on the ice, we normalize the $S(i)$ so that $S(1) = 1$; i.e. there is no beam spreading for the surface reflection.

The above-described numerical method for obtaining reflection profiles was carried out on the computer at Dartmouth College, Hanover, New Hampshire. We will now present the results of our calculations.

RESULTS

Anisotropic bottom reflections

Our calculations show anisotropic bottom reflections from sea ice at 100 MHz. Figure 8 gives the calculated reflection profiles of the two polarizations for the three

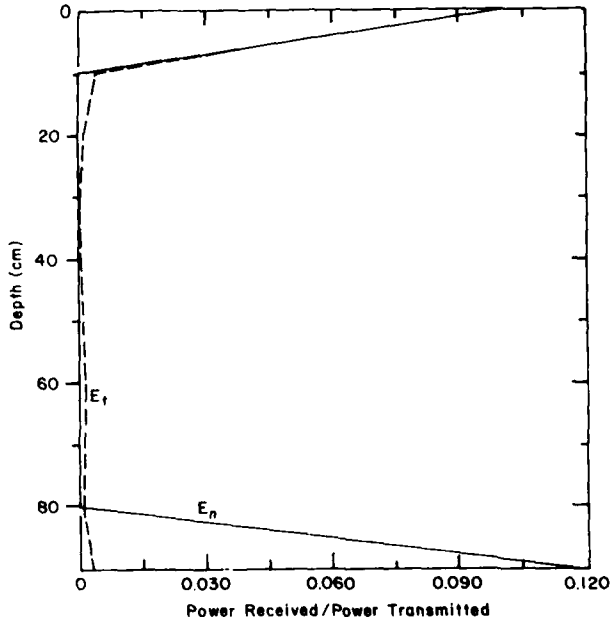

a. Cape Krusenstern (in the bottom layer $v_b = 0.17$).

Figure 8. Power reflection profile of $R_k(i)$ for Cape Kusenstern, Barrow and Harrison Bay. E_t denotes tangential polarization, E_n denotes normal polarization.

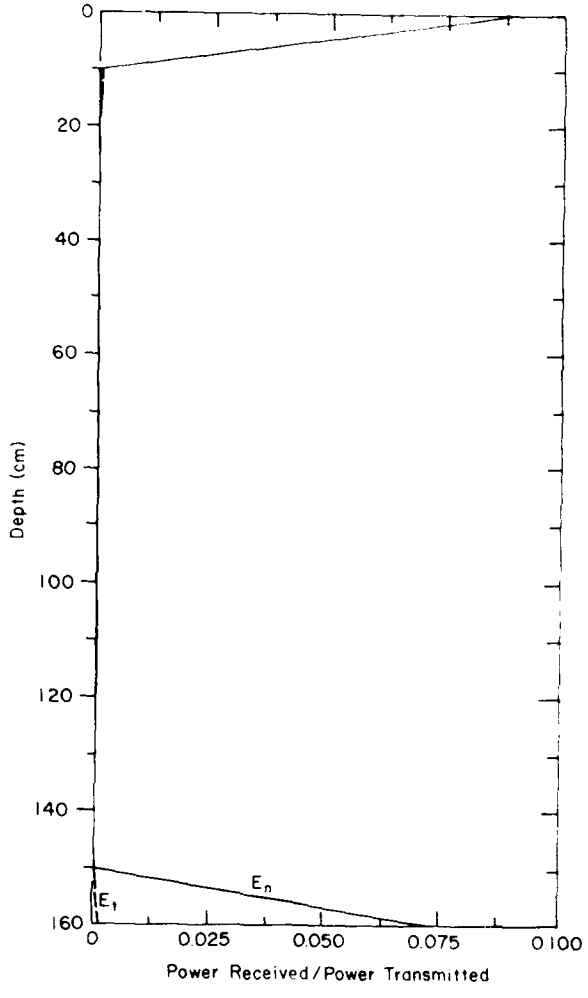

b. Barrow (in the bottom layer $v_b = 0.12$).

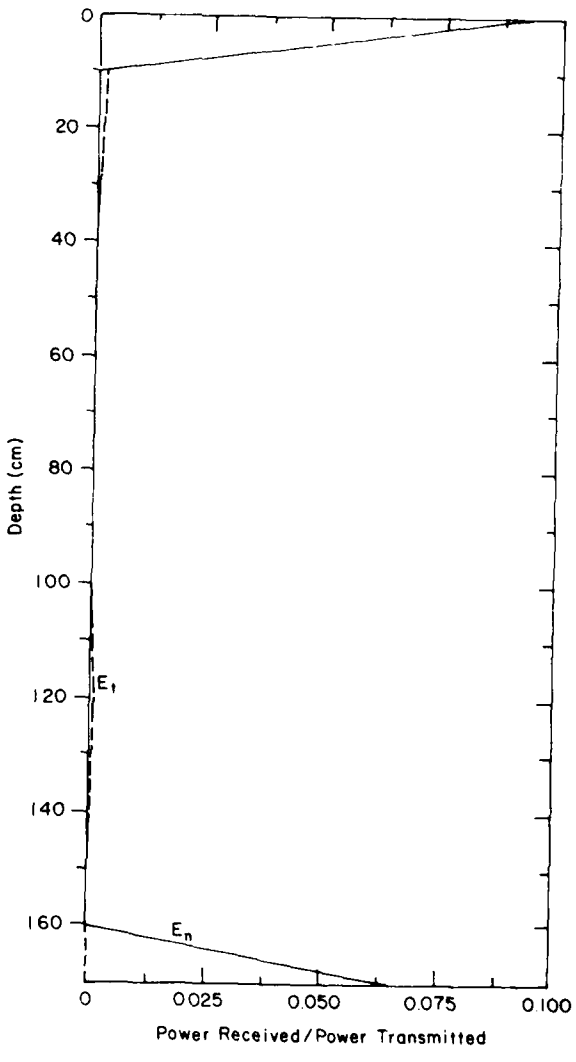

c. Harrison Bay (in the bottom layer $v_b = 0.29$).

Figure 8 (cont'd).

Table 1. Bottom reflection anisotropies.

Site	$v_b(1-d/2)$	K'	K
Cape Krusenstern	0.17	2.2	41
Barrow	0.12	1.9	56
Harrison Bay	0.29	3.0	800

sites. Table 1 gives the bottom layer brine volume, the coefficient of anisotropy for interfacial bottom reflection $K' = R'_n(n)/R'_t(n)$, and the coefficient of anisotropy for net bottom reflection $K = R_n(n)/R_t(n)$ for each site. Note the correlation between bottom layer brine volume and bottom interfacial anisotropy in Table 1. This is not the case for K since net reflections are determined by attenuation and reflections above the bottom interface.

Anisotropic complex dielectric constants

In our numerical model, reflective anisotropy can only exist with anisotropic dielectric constants. Figure 9 shows the dielectric constant profiles at Harrison Bay for both normal and tangential polarizations. The anisotropy is most pronounced in the lower region of the ice where the brine volume and a/b ratio are high, i.e. where the brine layers are numerous and well-defined. The wave is highly attenuated in these lower regions

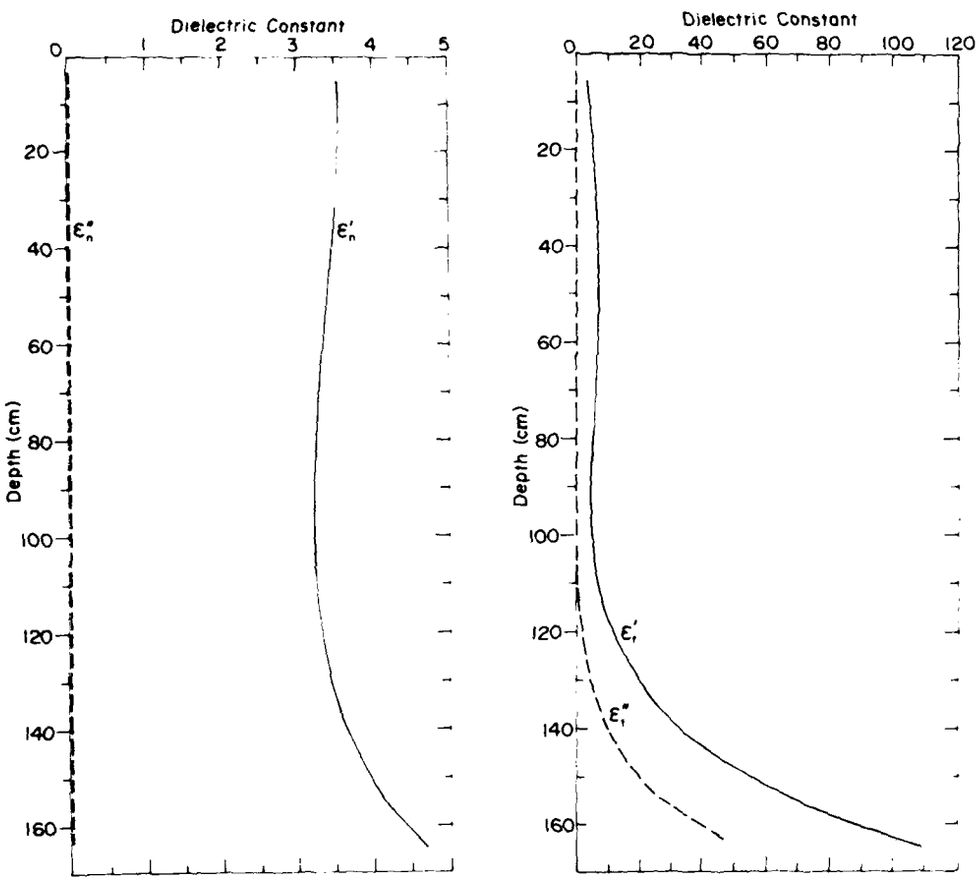

a. Normal polarization. *b. Tangential polarization.*

Figure 9. Real and imaginary parts of the complex mixture dielectric constants at Harrison Bay.

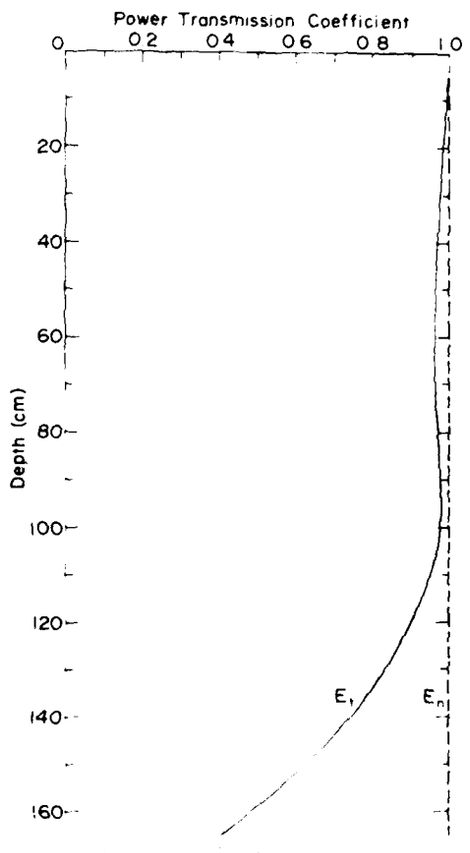

Figure 10. One-way power transmission coefficients for normal (E_n) and tangential (E_t) polarization at Harrison Bay. Low transmissions through the layers indicate high attenuation.

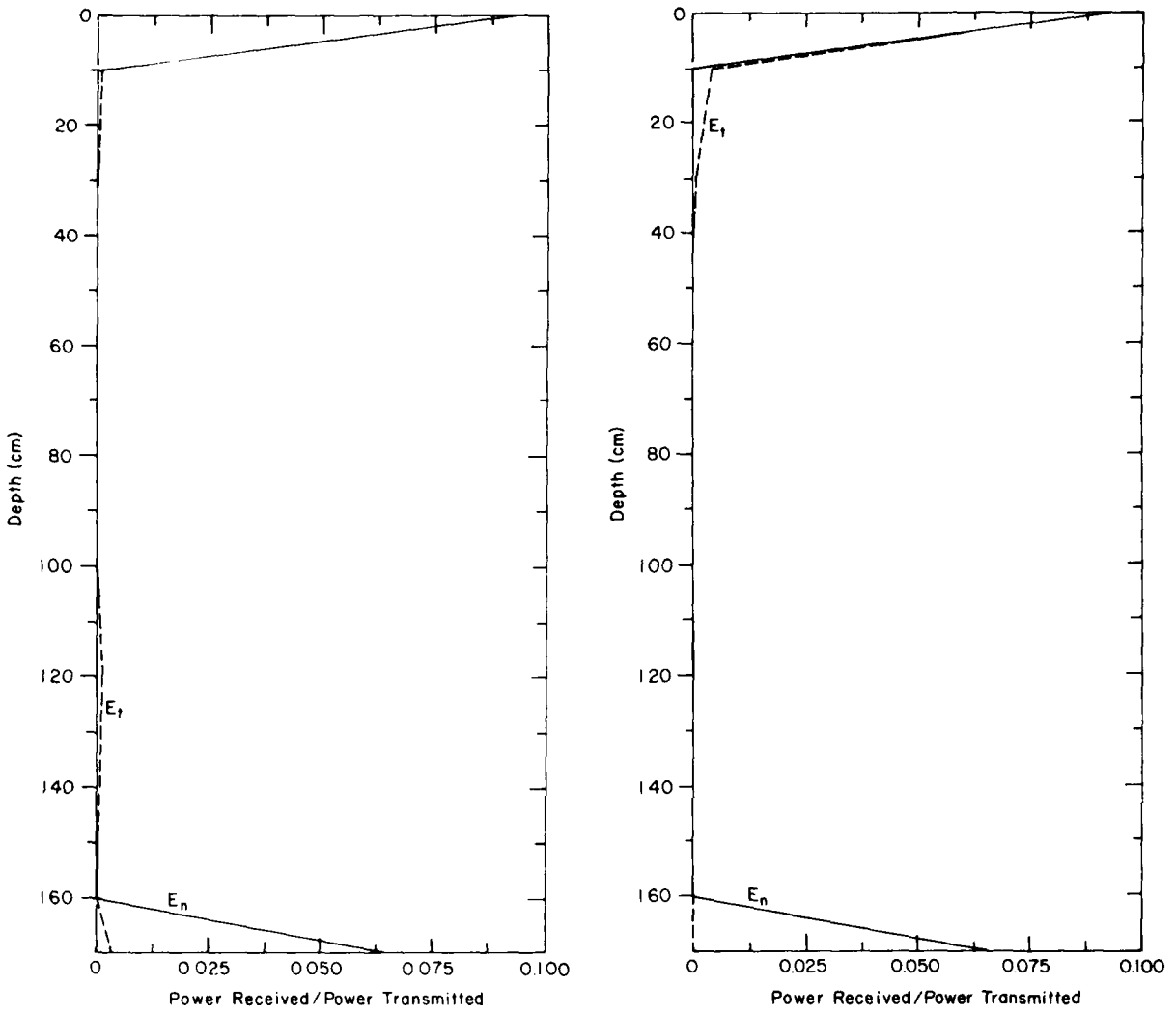

a. a:b:c = 20:1:5 at bottom.

b. a:b:c = 50:1:5 at bottom.

Figure 11. Power reflection coefficient $R_k(i)$ *profiles at Harrison Bay.*

because of the very large contribution of ϵ'' for tangential polarization, as suggested previously. Figure 10 shows the one-way power transmission coefficients $|e^{-\alpha(i)d}|^2$ for Harrison Bay associated with this attenuation. The ratio of the imaginary dielectric constants for the bottom layer at this site, $\epsilon_t''/\epsilon_n'' = 47.3/0.027 \approx 1800$ is roughly in agreement with the ratio of power losses in eq 13, $W_t/W_n \approx 2200$, the calculation of which was based on normal exclusion and tangential penetration of electric flux.

We see that the real part of the complex mixture dielectric constant for tangential polarization at the bottom of the ice at Harrison Bay has become quite high (109), in fact higher than that of brine itself (80). The finite extent of the brine layers causes them to behave as macroscopic dipoles. Free and polarization charges can build up at the ends of the brine layers, rendering the sea ice highly polarizable, more so than pure brine with no interfaces.

The combination of the large real and imaginary parts of the mixture dielectric constant for tangential polarization cause the bulk impedance of the bottom sea ice layer to be similar to that of the water below. Consequently, after downward propagation, the remaining energy of the tangentially polarized wave tends to be transmitted, rather than reflected at the ice/water interface, as is shown in Table 1 by the K'. The normally polarized wave encounters an impedance mismatch and is reflected.

Sensitivity of parameters

If one holds axes *b* and *c* constant while decreasing

a, the anisotropy decreases. Figure 11a gives the reflection profile for bottom $a:b:c$ = 20:1:5. The increase in bottom return for tangential polarization is due to the increase in surface area of the ellipsoids presented normally to the field, which results in less electric flux penetration and less attenuation, as has been previously shown. If the a axis is increased, as in Figure 11b where the bottom axial ratios are $a:b:c$ = 50:1:5, then the return of the tangentially polarized wave is decreased primarily because of higher attenuation from increased flux penetration into the brine layers. Note that the bottom return for normal polarization is constant for Figures 8c, 11a and 11b since electric flux is effectively excluded from the brine layers in all cases.

If one holds axes a and b constant while increasing c, the anisotropy decreases; the bottom return for tangential polarization increases while that for normal polarization stays constant. The reasoning for this effect is the same as that above: an increase in c (like a decrease in a) allows a larger depolarizing field to be created in the ellipsoid so that less of the wave will be attenuated. Decreasing the layer thickness d smooths the impedance mismatches at interfaces within the sea ice and thus decreases the magnitudes of the interfacial reflection coefficients.

Internal reflection: the bumps

It is very interesting to note the appearance of an internal reflection located at a depth of about $2T/3$ (Fig. 8a, 8c, and 11a) for tangential polarization. *In the model* this bump arises from a superposition of two effects. A large brine volume gradient and an increase in axial ratio with depth first combine to create impedance mismatches between layers, with resulting interfacial reflections starting up in the ice sheet and extending downward to the bottom. When the ice slab is very lossy at the bottom (for example, when $a:b:c$ = 30:1:5) the bottom reflections are cut out by attenuation, leaving the bump higher in the ice sheet (Fig. 8c). The position of the bump may be moved lower in the ice sheet by varying the axial ratio function with depth so that larger a/b ratios are not encountered until the lowest portions of the ice sheet, e.g. $f(z) = \alpha + \beta/(z - T)$, where α and β are constants used to fit the boundary conditions of isotropy near the top and maximal anisotropy near the bottom.

Kovacs and Morey (1979) have postulated the existence of this bump in explaining how reflective anisotropy can coexist with travel-time (and apparent dielectric constant) isotropy. They hypothesize that the reflection associated with the bump of tangential polarization (which they term an upward shift of the electromagnetic boundary) appears as a small bottom reflection since the higher dielectric constant of the ice for tangential polarization causes the wave velocity to decrease. Figure 4 of Campbell and Orange (1974) can be interpreted to show return higher in the ice sheet when the antenna is oriented for minimum bottom reflection. We leave this very interesting aspect of the reflective anisotropy open to more exhaustive experimentation.

DISCUSSION

We have assumed extreme order in the microstructure of sea ice. Effective axial ratios for brine inclusions at a given depth or region within sea ice are most probably distributed about some mean, and there is certainly variation in the orientations of the brine inclusions. However, the standard deviations for the preferred bottom c-axis azimuth given by Weeks and Gow (1979) are between 5° and 15°, indicating a higher degree of ordering. Our purpose was to show that if one views brine inclusions as finite, anisotropic, conducting bodies that are small compared to wavelength, then the observed reflective anisotropy follows naturally from the behavior of the electromagnetic field around and in the bodies, as specified by Maxwell's equations. To better illustrate mechanisms determining reflective anisotropy, we have taken a simplified model of sea ice. Examination of these limiting cases may render the observed data more understandable.

For instance, in our theoretical explanation of reflective anisotropy we concern ourselves primarily with a limiting case of brine structure, namely brine layers (Fig. 3a, b). Throughout much of the ice sheet, the brine structure takes the form of rows of vertical, cigar-shaped inclusions with a top view similar to that in Figures 3c and 3d. However, even if there is no horizontal anisotropy in the inclusion ($a:b:c$ = 1:1:5), there will be an anisotropy in electric flux penetration, as long as the distance between adjacent inclusions is less than the distance between adjacent rows of inclusions. During normal polarization, induced dipoles interact so that in the region between adjacent inclusions where the electric field is tangential to the surface, flux is diminished. Consequently, penetration of the field into the "cigars" for normal polarization is less than that for tangential polarization, as long as the above distance relations are kept. However, reflective anisotropy associated with these ordered "cigars" will be smaller than that associated with the brine layers.

An initial impetus for the present research was our dissatisfaction with the parallel plate waveguide model proposed by Kovacs and Morey (1978) to explain the anisotropy phenomenon. In this model, the brine

structure near the bottom of the ice is assumed to behave as a parallel plate waveguide. The frequency of 100 MHz is well below cutoff for the waveguide, so that attenuation rather than propagation exists for polarization parallel to the plates. The most fundamental problem with this theory is the lack of evidence for the existence of well-defined plates of the type required by their arguments. We feel that it is more natural to consider the brine structure as consisting of individual, finite, anisotropic bodies rather than continuous plates.

CONCLUSIONS

The reflective anisotropy observed in sea ice can be explained by consideration of the geometrical asymmetries inherent in the brine structure of sea ice with a high azimuthal order of *c*-axis orientation. Axial ratios of the brine layers of the order of 30:1:5 give a reasonable level of power returned to the ice surface in the direction normal to the brine layers (parallel to the *c*-axis) while significantly attenuating the power tangential to the brine layers (perpendicular to the *c*-axis).

The reflective anisotropy is understood by considering the amount of electric field that penetrates the brine layers for the tangential and normal polarizations. Large electric field penetration in the tangential case allows conduction effects to attenuate the wave and reduce the power returned from the ice/water interface. Impedance matching at the ice/water interface in the tangential case also allows more of the incident power to penetrate into the sea water instead of being reflected by the interface.

The parameters of interest for the magnitude of the reflected power in the model calculations are the brine volume profile with depth and the axial ratios of the brine inclusions relative to the polarization of the wave. Variation in these parameters during model calculations indicated that reflection profiles would be substantially changed by the imposed variations. Further experimental work relating the observed reflected power to the details of the sea ice microstructure (the axial ratio variations and distributions with depth, and brine volume information) could be used to establish one-to-one relationships between power levels returned from certain depths and ice microstructure. If these relationships can be established, radar sounding of sea ice could then be used as a nondestructive "spectroscopic" tool, giving information on the microstructure variations that ultimately control the strength and other important physical properties of sea ice. At present, microstructure information can only be obtained by coring a small sample of ice. A methodology that could extend this information to line and area measurements such as radar sounding would be valuable in future engineering and scientific investigations of sea ice.

LITERATURE CITED

Anderson, D.L. and W.F. Weeks (1958) A theoretical analysis of sea ice strength. *Transactions, American Geophysical Union*, vol. 39, no. 4, p. 632-640.

Campbell, K.J. and A.S. Orange (1974) The electrical anisotropy of sea ice in the horizontal plane. *Journal of Geophysical Research*, vol. 79, no. 3, p. 5059-5063.

Cherepanov, N.V. (1971) Spatial arrangement of sea ice crystal structure (in Russian). *Problemy Arktiki Antarktiki*, vol. 38, p. 137-140. (English translation, National Technical Information Service, Springfield, Va.)

Hargreaves, N.D. (1977) The polarization of radio signals in the radio echo sounding of ice sheets. *Journal of Physics, D: Applied Physics*, vol. 10, p. 1285-1301.

Hobbs, P.V. (1974) *Ice physics*. Oxford: Clarendon Press.

Jackson, J.D. (1975) *Classical electrodynamics*. New York: John Wiley and Sons.

Johari, G.P. and P.A. Charette (1975) The permittivity and attenuation in polycrystalline and single-crystal ice Ih at 35 and 60 MHz. *Journal of Glaciology*, vol. 14, no. 71, p. 293-303.

Kovacs, A. and R.M. Morey (1978) Radar anisotropy of sea ice due to preferred azimuthal orientation of the horizontal *c*-axes of ice crystals. *Journal of Geophysical Research*, vol. 83, no. C12, p. 6037-6046.

Kovacs, A. and R.M. Morey (1979) Anisotropic properties of sea ice in the 50-150 MHz range. *Journal of Geophysical Research*, vol. 84, no. C9, p. 5749-5759.

Kraus, J.P. (1953) *Electromagnetics*. New York: McGraw-Hill.

Lorrain, P. and D.R. Corson (1970) *Electromagnetic fields and waves*. San Francisco: W.H. Freeman.

Reitz, J.R. and F.J. Milford (1967) *Foundations of electromagnetic theory*. Reading, Massachusetts: Addison-Wesley Publishing Co.

Stratton, J.A. (1941) *Electromagnetic theory*. New York: McGraw-Hill.

Tiller, W.A. (1964) Dendrites. *Science*, vol. 146, no. 3646, p. 871-879.

Tinga, W.R., W.A.G. Voss and D.F. Blossey (1973) Generalized approach to multiphase dielectric mixture theory. *Journal of Applied Physics*, vol. 44, no. 9, p. 3897-3902.

van de Hulst, H.C. (1957) *Light scattering by small particles*. New York: John Wiley and Sons.

Vant, M.R. (1976) A combined empirical and theoretical study of the dielectric properties of sea ice over the frequency range 100 MHz to 40 GHz. Ph.D. thesis, Carleton University, Ottawa, Ontario (unpublished).

von Hipple, A.R. (1954) *Dielectrics and waves*. Cambridge, Massachusetts: MIT Press.

Ward, S.H. (1967) Electromagnetic theory for geophysical applications. In *Mining Geophysics*. Tulsa, Oklahoma: Society of Exploration Geophysicists.

Weeks, W.F. and A. Assur (1967) The mechanical properties of sea ice. CRREL Monograph II-C3. AD 662716.

Weeks, W.F. and A.J. Gow (1979) Crystal alignments in the fast ice of arctic Alaska. CRREL Report 79-22. ADA077188.

Golden, Kenneth M.
Modeling of anisotropic electromagnetic reflection from sea ice / by Kenneth M. Golden and Stephen F. Ackley. Hanover, Hanover, N.H.: U.S. Cold Regions Research and Engineering Laboratory; Springfield, Va.: available from National Technical Information Service, 1980.
vi, 15 p., illus.; 28 cm. (CRREL Report 80-23.)
Prepared for National Science Foundation by Corps of Engineers, U.S. Army Cold Regions Research and Engineering Laboratory under Grant DPP77-24528.
Bibliography: p. 15.
1. Anisotropy. 2. Electromagnetic wave reflections. 3. Mathematical models. 4. Sea ice. I. United States. Army. Corps of Engineers. II. Army Cold Regions Research and Engineering Laboratory, Hanover, N.H. III. Series: CRREL Report 80-23.

U S GOVERNMENT PRINTING OFFICE 1980—700-418 250